Journal of the Mechanics and Physics of Solids 73 (2014) 151–165

Contents lists available at ScienceDirect

Journal of the Mechanics and Physics of Solids

journal homepage: www.elsevier.com/locate/jmps

Cooperative entry of nanoparticles into the cell

Jiuling Wang [a], Haimin Yao [b], Xinghua Shi [a,*]

[a] The State Key Laboratory of Nonlinear Mechanics, Institute of Mechanics, Chinese Academy of Sciences, China
[b] Department of Mechanical Engineering, The Hong Kong Polytechnic University, Hung Hom, Kowloon, Hong Kong SAR

ARTICLE INFO

Article history:
Received 29 April 2014
Received in revised form
9 September 2014
Accepted 17 September 2014
Available online 28 September 2014

Keywords:
Cellular uptake
Nanoparticles
Cooperative entry
Spherical buds
Theoretical work

ABSTRACT

Interaction of nanoparticles (NPs) with cell membrane is a crucial issue in studying drug delivery, photodynamic therapy system and cytotoxicity. Single NP with relatively small size cannot be fully wrapped by the cell membrane, which prohibits its uptake. One feasible way is cooperative entry, i.e., recruiting and assembling multiple small NPs to form a larger NP cluster to enter into a cell. In this work, we present theoretical analysis about the cooperative entry of multiple NPs. Through free energy calculation we investigate how the NPs' size, shape, interval and NP/cell interfacial binding energy influence the feasibility of entry. Interestingly we find that the cooperative entry of oblate ellipsoidal NPs can get larger energy compensation than individual ones as well as spherical ones. We also propose that soft NPs have preference in cooperative entry of the cell. Our work can be used to actively design and transfer NPs in applications such as drug delivery as well as to understand the shape effect on toxic mechanism of ellipsoidal NPs.

1. Introduction

While showing toxic effect to cells (Lewinski et al., 2008; Shi et al., 2011), nanoparticles (NPs) have also proved to be important loading vehicles for drug delivery and bioimaging in biomedical applications (Davis et al., 2008; Doane and Burda, 2012; Slowing et al., 2008). Since the critical step for NPs' uptake is to cross the cell membrane, understanding the interaction between NPs and cell membrane thus becomes important. During the past few years, extensive experimental and theoretical works have been conducted to investigate the NPs/cell interaction with focus on the effect of particle size, shape, elasticity and surface physicochemical properties. For instance, Osaki et al. (2004) found the cell preferred to uptake NPs of diameter 50 nm. The mechanism of such size dependence was then elucidated by Gao et al. (2005) with a receptor-mediated endocytosis model and Zhang et al. (2009) with a thermodynamic model. The shape effects of NPs in phagocytosis (Champion and Mitragotri, 2006) and receptor-mediated endocytosis (Agarwal et al., 2013; Chithrani et al., 2006; Florez et al., 2012; Gratton et al., 2008) were also verified experimentally and theoretically (Yang and Ma, 2010). It is worth noting that in receptor-mediated endocytosis, the cell did not favor NPs with high aspect ratio, which is due to the high energy consumption induced by membrane wrapping in the region of NPs with large curvature. Consequently it is found that the elasticity of NPs played significant role in cellular uptake of NPs (Yi et al., 2011). Such elasticity dependent uptake was attributed to the shape transformation of NPs from sphere to ellipsoid during uptake, which resulted in high energy consumption for cells to fully wrap the NPs.

* Corresponding author.
E-mail address: shixh@imech.ac.cn (X. Shi).

http://dx.doi.org/10.1016/j.jmps.2014.09.006
0022-5096/

Despite these progresses which focus on the interaction of cells with individual NP, relatively few works investigate the cell interacting with multiple NPs. It is known that to fully wrap a spherical NP, the bending energy cost of membrane, $8\pi\kappa$, is independent of the size of NP, where κ is the bending rigidity of membrane (Deserno, 2004). However, the binding energy between the NP and membrane, which is the driving force for the NP to be internalized, decreases with the size of NP. It is natural to question how the NP could be fully wrapped and internalized when the size is smaller than the critical value estimated to be about 20 nm (Zhang et al., 2009). In a molecular simulation work, Reynwar et al. (2007) have demonstrated that specialized proteins could aggregate and create membrane curvature, which eventually triggers tubulation and forms vesicle. They have proposed that the cooperative action of proteins in binding the membrane is essential for such vesicle budding. Following this work, Yue and Zhang (2012) have investigated the cooperative effects in receptor-mediated endocytosis of multiple NPs. Qualitatively they have found that small NPs generally cluster into a close packed aggregate and are internalized as a whole. This finding is actually consistent with the experimental observation that small gold NPs with diameter of 14 nm apt to cluster together before uptake (Chithrani and Chan, 2007). In order to uncouple the complex interactions between NPs and membrane, Jaskiewicz et al. (2012a, 2012b) have used polymersomes as model membranes to investigate internalization of silica NPs. They have found that silica NPs with radius of 14 nm would internalize into the polymersomes as a cluster (Jaskiewicz et al., 2012b). Using numerical simulations, Bahrami et al. (2012) and Saric and Cacciuto (2012a, 2012b) have studied the linear aggregation and tube formation of multiple spherical NPs adsorbed on vesicles, which is a specialized case of NPs' clustering. These findings have provided a guidance to elucidate how small NPs enter the cell. However, the influences of particle interval distance, membrane tension, interfacial binding energy etc. have not been well studied, and the effects on cellular uptake are still far away from being conclusive. Furthermore, the geometry effect is not considered in these works, which has been proved to play an important role in cellular uptake of single NP (Bahrami, 2013; Champion and Mitragotri, 2006; Dasgupta et al., 2013, 2014; Decuzzi and Ferrari, 2008; Florez et al., 2012; Gao, 2014; Wang et al., 2013; Yang and Ma, 2010; Yi and Gao, 2014; Yi et al., 2014).

In this work, we present a thermodynamic model to describe the cooperative entry of multiple NPs into the cell. Following the Canham–Helfrich's framework (Helfrich, 1973), we systematically investigate how NP size, NP separation, membrane tension, interfacial binding energy and shape of NPs influence the uptake. The rest of this paper is organized as follows. In Section 2, a theoretical model is set up with the numerical simulation method described. The results for spherical, ellipsoidal, cylindrical and elliptic cylindrical NPs are presented and discussed in Section 3. Section 4 summarizes the results and findings.

2. Model and methods

2.1. Energy contribution

When multiple NPs adhere to an initially flat membrane, the membrane deforms and engulfs a group of NPs by one spherical vesicle, which is a common process in cellular endocytosis (Canton and Battaglia, 2012). Before the vesicle is pinched off from the cell membrane to complete the internalization, the system with multiple NPs engulfed by the vesicle could be considered as a final state of NP/membrane interaction. Fig. 1a shows a model system with spherical vesicle wrapping multiple identical NPs. To describe the problem conveniently, we assume the NPs are uniformly distributed on the vesicle and the total number of NPs within the vesicle is approximately given by

$$n=\frac{4\pi R^2}{2\pi R^2(1-cos\varphi)}=\frac{2}{1-cos\varphi}, \tag{1a}$$

for 3D case and

$$n=\frac{\pi}{\varphi}, \tag{1b}$$

for 2D case, where φ is the half-central angle for individual NP. With this assumption, the spherical vesicle could be allocated into n patches with each patch interacting with one NP, as shown in Fig. 1b. In what follows we will only consider one NP interacting with the membrane. We note that topologically the surface of a sphere cannot be equally divided into n patches, and Eq. (1) is adopted here for mathematical convenience. Following the Canham–Helfrich's framework (Helfrich, 1973), the total free energy of the system consists of bending energy, tension energy, adhesion energy and work of pressure difference, which is described as

$$E=E_b+E_a+E_t+\Delta P\Delta V, \tag{2}$$

where E_b, E_a and E_t represent bending energy of membrane, NP/membrane interfacial adhesion energy and tension energy of membrane, respectively. ΔP is the osmotic pressure difference and for simplicity, we set $\Delta P=0$, i.e. the osmotic pressure difference between inside and outside of the cell membrane is zero.

In this model, we adopt a symmetric membrane and assume no topological change during the whole process. Then according to the Canham–Helfrich's fluid membrane model (Helfrich, 1973), the bending energy for each NP is given by

$$E_b=\int_S\frac{\kappa}{2}(c_1+c_2)^2dS, \tag{3}$$

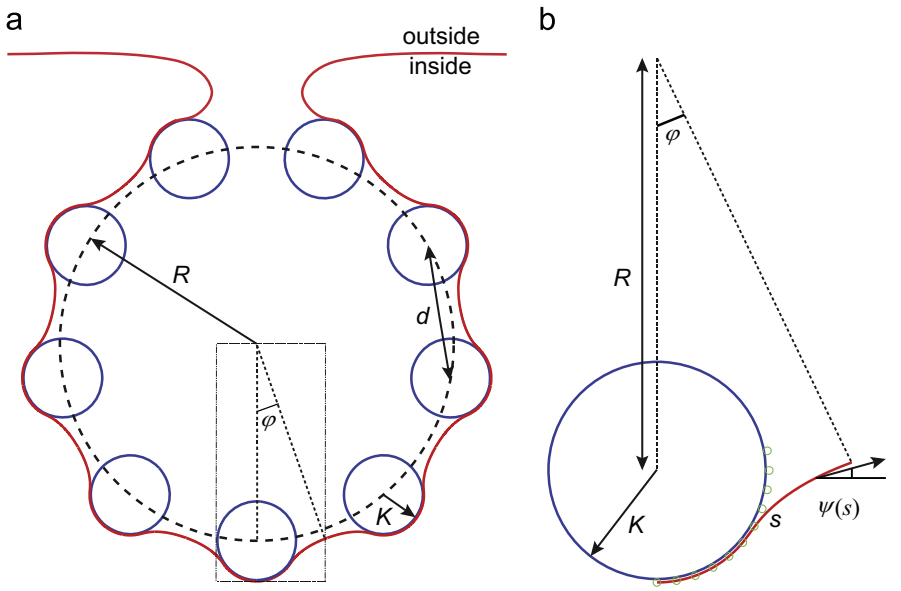

Fig. 1. (a) The schematic shows of cellular uptake of multiple spherical NPs. K is the radius of spherical NPs, R is the radius of spherical vesicle, d is NPs separation, and φ is half-central angle of individual NP. (b) A local amplification of (a). $\psi(s)$ is the angle tangent to the profile. This figure represents 3D and 2D cases.

where κ is the bending rigidity of membrane, and c_1 and c_2 are principal curvatures of the membrane surface. The tension energy is given by

$$E_t = \sigma \Delta S, \tag{4}$$

where σ is the surface tension of the membrane and ΔS the excess surface area induced by wrapping NPs. Different from conventional adhesion energy calculation which is obtained by adhesion strength multiplying contact area, here we adopt 6-12 Lennard-Jones potential to calculate the adhesion energy (Jiang et al., 2006). Because the adhesion energy is mainly determined by material properties at the interfaces (Nel et al., 2009; Qin and Buehler, 2014; Verma and Stellacci, 2010), we get the adhesion energy by integrating the Lennard-Jones potential over surface atoms, which is given by

$$E_a = \int \rho_m dS_m \int V(r)\rho_p dS_p, \tag{5}$$

where ρ_m and ρ_p are respectively atom densities of the membrane and the particle surface, dS_m and dS_p are elements of membrane and particle surface, respectively, and $V(r)$ is Lennard-Jones potential between atoms on membrane and particle surface with the expression

$$V(r) = 4\varepsilon\left(\frac{\sigma_{lj}^{12}}{r^{12}} - \frac{\sigma_{lj}^{6}}{r^{6}}\right), \tag{6}$$

where ε and σ_{lj} are Lennard-Jones parameters and r the distance between two atoms.

2.2. Parameterization of the membrane profile

In order to parameterize the profile of the membrane, we select arc length s and angle $\psi(s)$, the angle tangent to the profile, as coordinate axes. Set $s = 0$ at the initial point of the profile, we assume that $\psi(s)$ has a Fourier series form with respect to arc length s (Gozdz, 2007)

$$\psi(s) = \frac{\varphi}{L}s + \sum_{i=1}^{N} a_i \sin\left(\frac{\pi}{L}is\right), \tag{7}$$

where a_i is Fourier amplitude and L the total arc length of the membrane profile. Gozdz (2007) has used this method to explore the deformations of lipid vesicles induced by an attached particle. The boundary condition is automatically satisfied, i.e. $\psi(0) = 0$ and $\psi(L) = \varphi$. While more terms would be better, we find after numerical tests that the profile of membrane could describe our problem well when $N = 20$. After parameterization, each part of energy can be expressed as

$$E_b = \pi\kappa \int_0^L r_s(s)\left[\frac{d\psi}{ds} + \frac{\sin\psi}{r_s(s)}\right]^2 ds, \tag{8}$$

$$E_t = \sigma \int_0^L 2\pi r_s(s) ds, \quad \text{with} \quad r_s(s) = \int_0^s \cos\ \psi ds \tag{9}$$

$$E_a = 16\pi^2 \rho_m \rho_p \varepsilon K^2 \int_0^L r_s(s) ds \int_0^{3\sigma_{lj}/K} \left[\frac{\sigma_{lj}^{12}}{r(s,\tau)^{12}} - \frac{\sigma_{lj}^{6}}{r(s,\tau)^{6}} \right] \sin\ \tau d\tau, \tag{10}$$

with

$$r(s,\tau) = \left\{ (K\ \sin\ \tau)^2 + \left[K(1-\ \cos\ \tau) + d(s) \right]^2 \right\}^{1/2}, \quad d(s) = \left[r_s(s)^2 + z_s(s)^2 \right]^{1/2} - K$$

where $r_s(s)$ is the distance between point s on membrane and the rotational axis, and $d(s)$ is the vertical distance between point s and spherical surface, with $z_s(s) = \int_0^s \sin\ \psi ds - (K+\delta)$, and δ is the distance between the membrane and the NP at point $s=0$. In Eq. (10), we have set the cutoff distance as $3\sigma_{lj}$ in adhesion energy calculation. The total energy E becomes the function of a_i and L when we replace $\psi(s)$ in Eqs. (8)–(10) by Eq. (7). In addition, the variables satisfy the following relationship

$$\varphi = atan\left[\frac{r_s(s)|_{s=L}}{R - z_s(s)|_{s=L}} \right]. \tag{11}$$

By performing energy minimization of the total energy under the constraint condition of Eq. (11), we will get parameters a_i and L, and accordingly the total energy E.

To reflect the intrinsic relationship among these parameters, here we construct several dimensionless parameters as follows (Deserno, 2004):

$$\nu = R/K,\ \ \overline{E} = E/(\pi\kappa),\ \ \overline{E}_b = E_b/(\pi\kappa),\ \ \overline{E}_t = E_t/(\pi\kappa),\ \ \overline{E}_a = E_a/(\pi\kappa),$$
$$\overline{\sigma} = \sigma K^2/\kappa,\ \ \overline{\varepsilon} = \varepsilon/\kappa,\ \ \overline{\sigma}_{lj} = \sigma_{lj}/K,\ \ \overline{\delta} = \delta/K,\ \ \overline{\rho} = \rho_m \rho_p K^4,\ \ \overline{P} = \Delta P K^3/\kappa \tag{12}$$

In present work, we consider NPs with radius of 15 nm, a typical membrane bending rigidity of 20 k_BT (Boal, 2012) and a membrane tension of 0.02 mN/m (Morris and Homann, 2001). Then the dimensionless parameter $\overline{\sigma} = \sigma K^2/\kappa$ would be about 0.055. Typical values of those parameters are listed in Table 1. The particle swarm optimization (PSO) algorithm is utilized to conduct the numerical optimization (Kennedy et al., 1995).

2.3. NPs with other shapes

To investigate the shape effect of NPs during uptake, ellipsoidal, cylindrical and elliptic cylindrical NPs are also investigated with the same method. For ellipsoidal NPs, we define a as the semi-major axis of the ellipsoid and b as semi-minor axis. The parameter K, the radius of spherical NP which has the same volume as the ellipsoid, is chosen as its equivalent particle size and defined as

$$K = \left(a^2 b\right)^{1/3}. \tag{13}$$

Here we only consider oblate ellipsoidal NP as shown in Fig. 2. We assume that $\psi(s)$ has the same form as shown in Eq. (7). Thus the bending energy and tension energy have the same expressions as spherical NPs. The adhesion energy is given by

$$E_a = 16\pi \rho_m \rho_p \varepsilon a^2 \int_0^L r_s(s) ds \int_0^{\pi} \left(cos^2\theta + \lambda^2 \sin^2\theta \right)^{1/2} d\theta \int_0^{\pi} \left[\frac{\sigma_{lj}^{12}}{r(\theta,\tau,s)^{12}} - \frac{\sigma_{lj}^{6}}{r(\theta,\tau,s)^{6}} \right] \sin\ \theta d\tau \tag{14}$$

where $\lambda = b/a$ is the aspect ratio

$$r(\theta,\tau,s) = \left\{ (a\ \sin\ \theta)^2 + r_s(s)^2 - 2a\ \sin\ \theta r_s(s) \cos\ \tau + \left[z_s(s) + b\ \cos\ \theta \right]^2 \right\}^{1/2},$$
$$r_s(s) = \int_0^s \cos\ \psi ds,\ \ z_s(s) = \int_0^s \sin\ \psi ds - (b+\delta).$$

Table 1
Parameters for spherical NPs.

Parameter	Numerical value
K (nm)	15
κ	$20k_BT$
ν	2–15
$\overline{\sigma}$	0.055
$\overline{\rho\varepsilon}$	541.7
$\overline{\sigma}_{lj}$	0.0313
$\overline{\delta}$	0.0313
$\overline{P}$	0

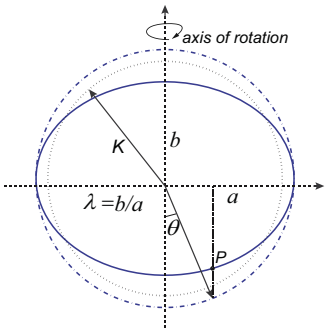

Fig. 2. The schematic shows an ellipsoidal NP. K is the equivalent particle size, λ is the aspect ratio, the coordinate of point P on the ellipsoid is expressed as $(a\ \sin\ \theta, -b\ \cos\ \theta)$.

The dimensionless parameters for ellipsoidal NPs are the same as spherical ones. To simplify the calculations, we also set the cutoff distance to $3\sigma_{lj}$. Part of parameters for ellipsoidal NPs is listed in Table 2 while the others are the same as that of spherical NPs.

For infinite long cylindrical NPs, the energy term per unit length for each NP is given as

$$E_b = \kappa \int_s (c_1+c_2)^2 ds = \kappa \int_0^L \left(\frac{d\psi}{ds}\right)^2 ds, \tag{15}$$

$$E_t = 2\sigma L, \tag{16}$$

$$E_a = 32\rho_m\rho_p\varepsilon K \int_0^L ds \int_0^{3\sigma_{lj}} dx \int_0^{3\sigma_{lj}/K} \left[\frac{\sigma_{lj}^{12}}{r(x,d,\tau)^{12}} - \frac{\sigma_{lj}^{6}}{r(x,d,\tau)^{6}}\right] d\tau, \tag{17}$$

where

$$r(x,s,\tau) = \left\{K^2 + [K+d(s)]^2 - 2K[K+d(s)]\ \cos\ \tau + x^2\right\}^{1/2},$$

$$d(s) = \left[r_s(s)^2 + z_s(s)^2\right]^{1/2} - K,$$

$$r_s(s) = \int_0^s \cos\ \psi ds,\ \ z_s(s) = \int_0^s \sin\ \psi ds - (K+\delta).$$

In Eq. (17), we have used the cutoff distance $3\sigma_{lj}$ for adhesion energy calculation. The dimensionless parameters for energy are different from 3D cases which are given by

$$\overline{E} = EK/\kappa,\ \ \overline{E_b} = E_bK/\kappa,\ \ \overline{E_t} = E_tK/\kappa,\ \ \overline{E_a} = E_aK/\kappa. \tag{18}$$

Parameters for cylindrical NPs are shown in Table 3 while the other parameters are the same as spherical NPs.

For elliptic cylindrical NPs, the bending and tension energy per unit length for each NP have the same expression as cylindrical NP, and the adhesion energy term per unit length for each NP is given as

$$E_a = 16\rho_m\rho_p\varepsilon a \int_0^L ds \int_{-3\sigma_{lj}/K}^{\pi} \left(cos^2\theta + \lambda^2 \sin^2\theta\right)^{1/2} d\theta \int_0^{3\sigma_{lj}} \left[\frac{\sigma_{lj}^{12}}{r(s,\theta,x)^{12}} - \frac{\sigma_{lj}^{6}}{r(s,\theta,x)^{6}}\right] dx \tag{19}$$

where

$$r(s,\theta,x) = \left\{[r_s(s) - a\ \sin\ \theta]^2 + [z_s(s) + b\ \cos\ \theta]^2 + x^2\right\}^{1/2},$$

$$r_s(s) = \int_0^s \cos\ \psi ds,\ \ z_s(s) = \int_0^s \sin\ \psi ds - (b+\delta).$$

The parameter K, the radius of cylinder which has the same section area as the elliptic cylinder, is chosen as the units of length and defined as

$$K = (ab)^{1/2}. \tag{20}$$

The dimensionless parameters constructed are the same as cylindrical NPs. Parameters for elliptic cylindrical NPs are shown in Table 4 while other parameters are the same as spherical NPs.

Table 2
Parameters for ellipsoidal NPs.

Parameter	Numerical value
$\overline{\rho\varepsilon}$	541.7 or 687.4
$\overline{\delta}$	0.0313

Table 3
Parameters for cylindrical NPs.

Parameter	Numerical value
$\overline{\rho\varepsilon}$	144.6
$\overline{\delta}$	0.0313

Table 4
Parameters for elliptic cylindrical NPs.

Parameter	Numerical value
$\overline{\rho\varepsilon}$	144.6 or 198.5
$\overline{\delta}$	0.0313

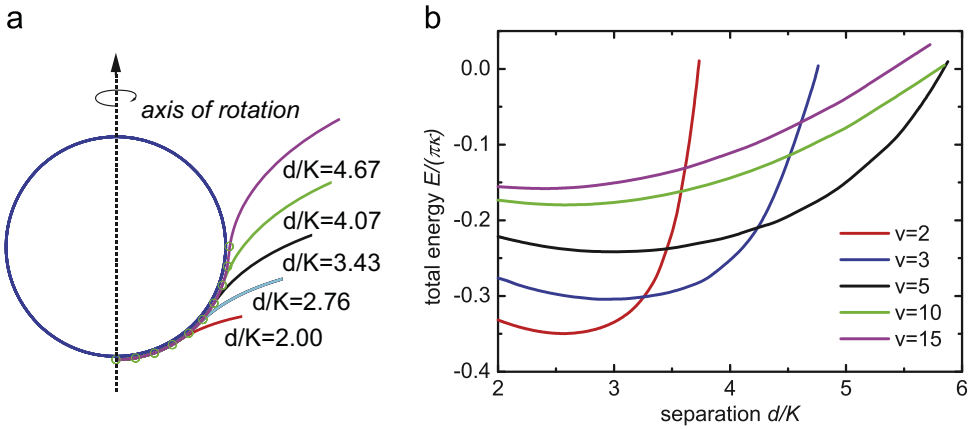

Fig. 3. (a) The membrane profiles with different NPs separation when the vesicle size is $v=5$. Green circles are used to guide the line of sight. (b) For spherical NPs, the energy profiles for different NPs separation with different vesicle sizes. This figure is for 3D case. (For interpretation of the references to color in this figure legend, the reader is referred to the web version of this article.)

3. Results and discussion

3.1. Spherical and ellipsoidal NPs (3D)

To investigate the effect of NPs separation as well as the vesicle size on uptake, we firstly fix the adhesion strength as $\overline{\rho\varepsilon}=541.7$. At this adhesion strength, the total energy would be about zero if cell membrane wraps individual NP completely. With the adhesion strength fixed, we get the membrane profile with different NPs separation when the vesicle size is $v=5$ (Fig. 3a). It is seen that the wrapping degree of membrane on NPs increases with the NPs separation. However, the relation for total energy with separation does not show such monotonic behavior. As shown in Fig. 3b, for a fixed size of vesicle v, the total energy E would first decrease then increase as the separation increases, which means there exists an optimal separation distance for uptake of multiple NPs. We note that the situation when NPs contact with each other ($d=2K$) is not the configuration having minimum energy. This is actually consistent with the work of Reynwar and Deserno (2011) and Reynwar et al. (2007).

In Fig. 4a, we show the optimal membrane profiles with different vesicle sizes for spherical NPs. The wrapping degree of membrane on NPs decreases as the vesicle size increases. Meanwhile, the total energy E at minimum would increase with

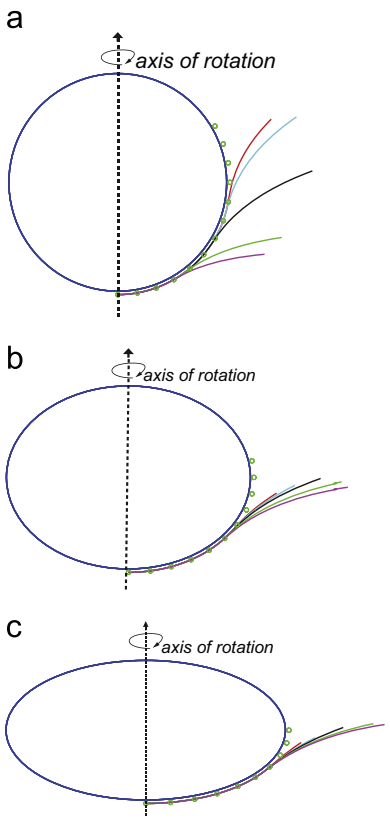

Fig. 4. (a) The optimal membrane profiles for spherical NPs with different vesicle sizes, red for $v=2$, cyan for $v=3$, black for $v=5$, green for $v=10$, purple for $v=15$. (b) The optimal membrane profiles for ellipsoidal NPs with $\lambda=0.75$, the different colors represent different vesicle sizes, which is the same as spherical ones. (c) The optimal membrane profiles for ellipsoidal NPs with $\lambda=0.5$, the color scheme is the same as in (b). This figure is for 3D case. (For interpretation of the references to color in this figure legend, the reader is referred to the web version of this article.)

the vesicle size as shown in Fig. 3b. It indicates the vesicle would energetically apt to be small one without considering the NPs interval distance.

To further identify how the NPs separation and vesicle size influence the system energy, we draw a phase diagram as shown in Fig. 5a. The dots in the figure represent the parameters with which the system has the lowest energy. It is seen that as the vesicle size increases, the optimized separation increases firstly then decreases, and finally tends to a constant value. And the separation is restricted within a small region around $2.5K$. It means during cooperative entry, the separation of NPs could not be too large. Otherwise one NP could not "sense" the other through the connection of membrane. This separation regulated cooperative entry may be important in biological system, since the interaction between NPs is universal, e.g. electrostatic interaction, which controls the final separation distance of NPs (Nel et al., 2009).

It has been demonstrated that the shape of NPs has key role in endocytosis (Agarwal et al., 2013; Champion and Mitragotri, 2006; Gratton et al., 2008; Yang and Ma, 2010). Here the ellipsoidal NPs with different aspect ratio λ are considered in cooperative entry. With the same adhesion strength as spherical NPs, there also exists an optimal NPs separation for ellipsoidal NPs. In Fig. 4b and c, we draw the optimal membrane profile on ellipsoidal NPs with different vesicle sizes. Different to spherical ones, the vesicle size has minor effect on the wrapping degree of membrane on ellipsoidal NPs ($\theta<60^\circ$). This is attributed to the small curvature in the contact region which induces less bending energy of membrane, thus compensates less adhesion energy. To analyze how the wrapping degree affects the bending energy of membrane, we deduce the mean curvature $M(\theta)$ of point P $(a\ \sin\ \theta, -b\ \cos\ \theta)$ on the ellipsoid

$$M(\theta)=\frac{c_1+c_2}{2}=\frac{\lambda}{2a}\frac{\left(1+\cos^2\theta+\lambda^2\sin^2\theta\right)}{\left(\cos^2\theta+\lambda^2\sin^2\theta\right)^{3/2}}. \tag{21}$$

When the NP surface within the region $[0,\theta]$ is wrapped by membrane, the bending energy cost is

$$E_b(\theta)=\frac{\kappa}{2}\int(c_1+c_2)^2dS=\pi\kappa\lambda^2\int_0^\theta \sin\ \theta\frac{\left(1+\cos^2\theta+\lambda^2\sin^2\theta\right)^2}{\left(\cos^2\theta+\lambda^2\sin^2\theta\right)^{5/2}}d\theta, \tag{22}$$

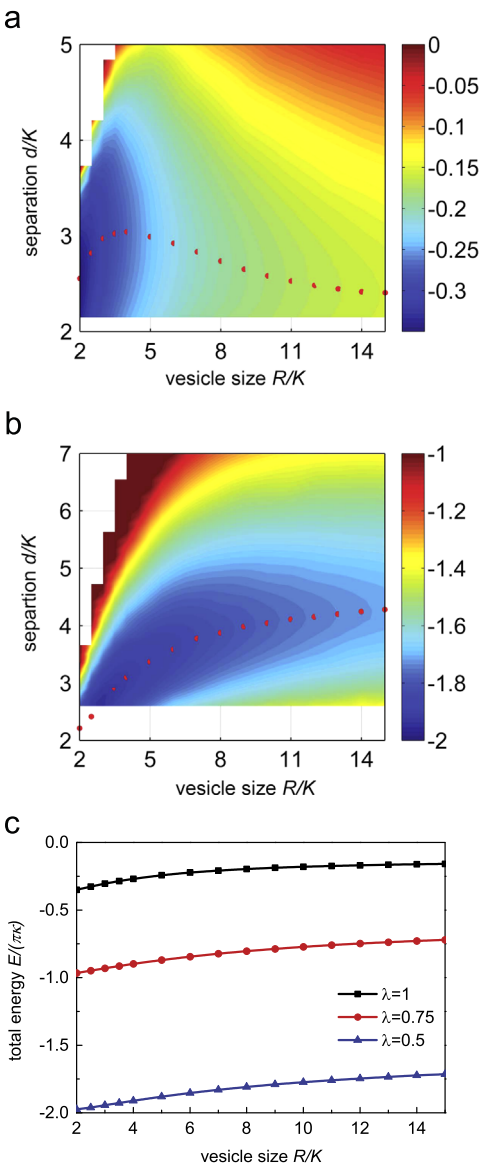

Fig. 5. A two-dimensional phase diagram characterizes effects of vesicle size and separation on the total energy for (a) spherical and (b) ellipsoidal NPs with $\lambda = 0.5$. The color bar indicates the level of dimensionless total energy. The red dots represent the separation with which the system has the lowest energy for a given vesicle size. (c) The variation of total energy with the vesicle size for different aspect ratios. The adhesion strength is $\overline{\rho\varepsilon} = 541.7$. This figure is for 3D case. (For interpretation of the references to color in this figure legend, the reader is referred to the web version of this article.)

where the surface area is

$$S(\theta) = 2\pi a^2 \int_0^{\theta} \sin\,\theta\left(\cos^2\theta + \lambda^2 \sin^2\theta\right)^{1/2} d\theta. \tag{23}$$

In Fig. 6a, we plot the mean curvature of the NPs surface as a function of wrapping degree. It seems that the mean curvature at the edges of the ellipsoidal NPs ($\theta = 90^\circ$) with $\lambda = 0.5$ is about $2/K$, double of that for spherical NPs ($\lambda = 1.0$). It means at this wrapping front, the bending energy cost is four times of that for spherical NPs. In Fig. 6b we plot the total bending energy cost as function of the wrapping degree. It is seen that the total bending energy cost increases as the aspect ratio decreases. Furthermore, for ellipsoidal NPs with $\lambda = 0.5$, the bending energy increases slowly as $\theta < 60^\circ$ while increases sharply as $\theta > 60^\circ$. That is why the wrapping degree of ellipsoidal NPs with $\lambda = 0.5$ is about 60°.

Compared with spherical NPs, ellipsoidal NPs gain significant energy compensation. As shown in Fig. 5b and c, with the same adhesion strength, the ellipsoidal NPs get larger energy gain than spherical ones. It is attributed to the fact that in the cooperative entry model, membrane does not need to wrap the strongly curved regions of ellipsoidal NPs. We also find the

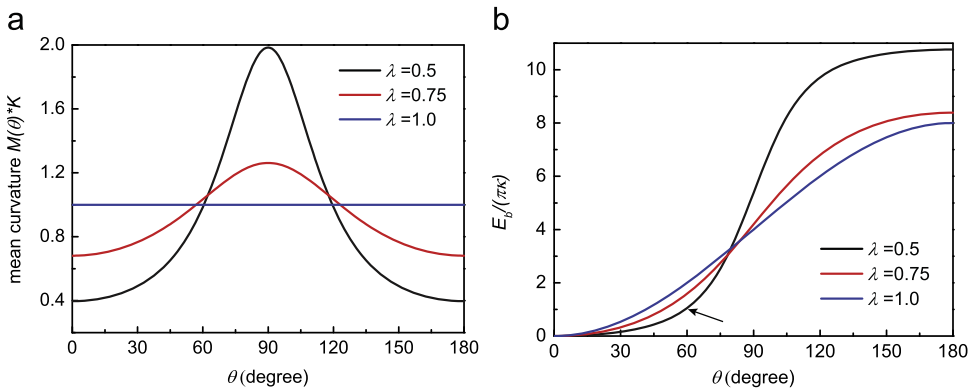

Fig. 6. (a) The mean curvature of the NPs surface as a function of θ and aspect ratio λ. (b) The bending energy cost of membrane as a function of wrapping degree with different aspect ratios of ellipsoidal NPs. The arrow indicates the wrapping front for ellipsoidal NPs with $\lambda = 0.5$. This figure is for 3D case.

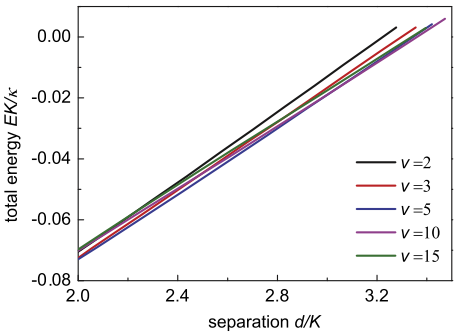

Fig. 7. Effects of the separtion on the total energy for cylindrical NPs with different vesicle sizes. This figure is for 2D case.

energy gain is large for small λ. It is attributed to the small bending energy cost as λ decreases. With the decrease of the aspect ratio, this trend will become more apparent.

3.2. Cylindrical and elliptic cylindrical NPs (2D)

Similar to spherical and ellipsoidal NPs (3D), we set up 2D model to describe the cooperative entry of infinite long cylindrical and elliptic cylindrical NPs with their axis parallel to the membrane. The adhesion strength is about $\overline{\rho\varepsilon} = 144.6$ for cellular uptake of individual cylindrical NPs completely. We assume the cell internalizes multiple cylindrical NPs by a tubular vesicle with circular cross-section as shown in Fig. 1a. In Fig. 7 we plot the total energy E versus cylindrical NPs separation with different vesicle sizes. Different from spherical NPs, the total energy increases linearly with respect to separation, and NPs would touch each other at the optimal configuration. Moreover, for different vesicle sizes the energy gain with the same separation is quite close. Note that here we do not consider the interaction between NPs (Chaudhuri et al., 2011).

For elliptic cylindrical NPs, they would not contact with each other at the optimal configuration except for vesicle size $v = 2$. Fig. 8a shows the vesicle size and the optimal separation with different sectional aspect ratios. For cylindrical NPs, the separation almost keeps to be a constant. For elliptic cylindrical NPs with $\lambda = 0.75$, the optimal separation region is between $2K$ and $3K$, which is small compared with the NPs with $\lambda = 0.5$. Hence the aspect ratio plays a significant role here. With the same adhesion strength, it is also insufficient to internalize single elliptic cylindrical NP. Via cooperative manner, however, it gets large energy gain as shown in Fig. 8b. This is because the membrane avoids the wrapping of strongly curved edges, which is similar to the case for ellipsoidal NPs.

3.3. Effect of adhesion strength

In order to understand the influence of adhesion strength, we have repeated the calculation with changed adhesion strength. Fig. 9a shows optimized NPs separation versus vesicle size at adhesion strength $\overline{\rho\varepsilon} = 687.4$ which is required for membrane to fully internalize individual ellipsoidal NPs with $\lambda = 0.5$. It is seen that the increase of adhesion strength by 27% would slightly change the separation (Fig. 9a) as well as the contact front (Fig. 10). The reason is the same as discussed above

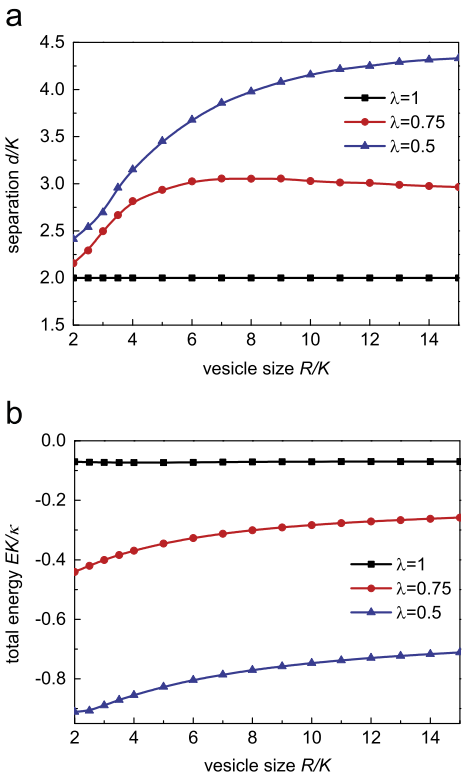

Fig. 8. (a) The vesicle size and optimal NPs separation at different NP's aspect ratios. (b) The variation of total energy with the vesicle size for different aspect ratios. This figure is for 2D case.

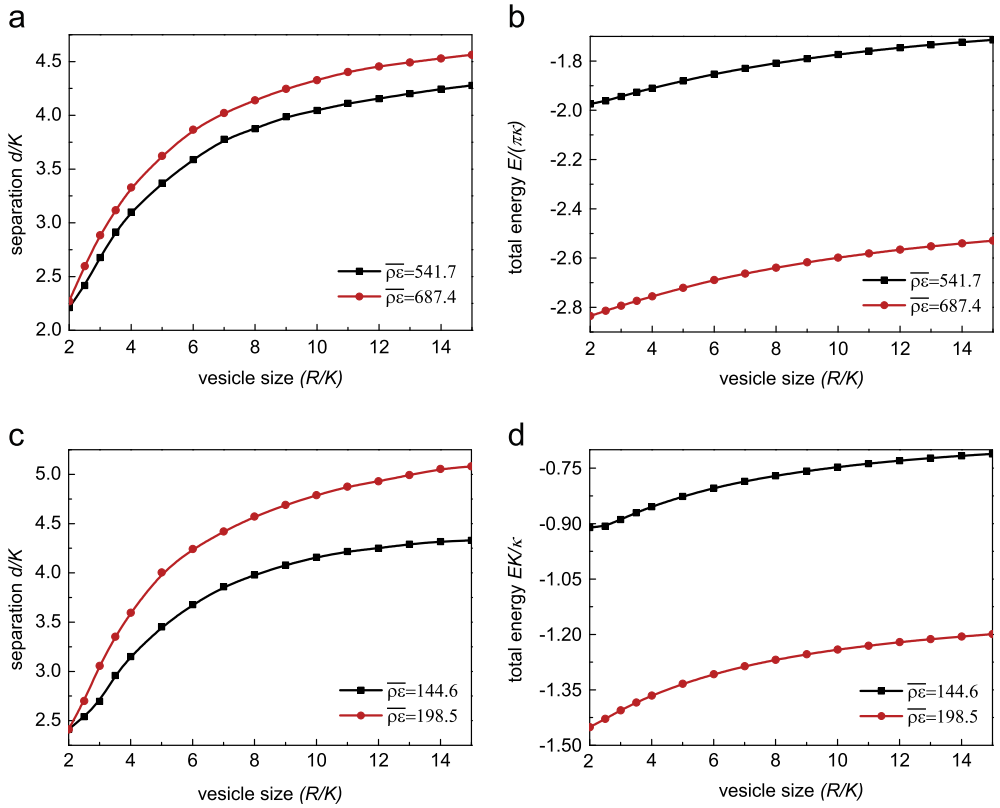

Fig. 9. Effects of the vesicle size on the separation (a) and the total energy (b) with different adhesion strengths for ellipsoidal NPs with $\lambda = 0.5$. (3D case) (c) and (d) are those for elliptic cylindrical NPs with sectional aspect ratio $\lambda = 0.5$ (2D case).

that wrapping the rest part of NPs, i.e. the strong curved edges, will cost abundant energy. The energy gain, however, increases by 40% with the increase of adhesion strength (Fig. 8b), indicating in the cooperative entry mode, the energy compensation would enhance greatly by increasing the adhesion strength. It is further proved that within a certain range of adhesion strength, cellular cooperative entry of multiple NPs has more advantages than entry of individual NP.

It shows similar results for elliptic cylindrical NPs when the adhesion strength is changed to $\overline{\rho\varepsilon} = 198.5$ which is required for cellular entry individual elliptic cylindrical NP with $\lambda = 0.5$. Fig. 9c and d shows the separation and total energy changes with the vesicle size.

3.4. Cutoff effect of adhesion potential

Different from the conventional method to calculate adhesion energy, here we adopt Lennard-Jones potential to characterize the interface adhesion energy where we set the cutoff distance as $3\sigma_{lj}$. It has been proved that the potential range would influence the result for cellular uptake NPs in a tubular mode (Bahrami et al., 2014; Raatz et al., 2014). To check the effect of cutoff distance in our model, we have repeated the calculation by increasing the cutoff distance to $5\sigma_{ij}$. Fig. 11

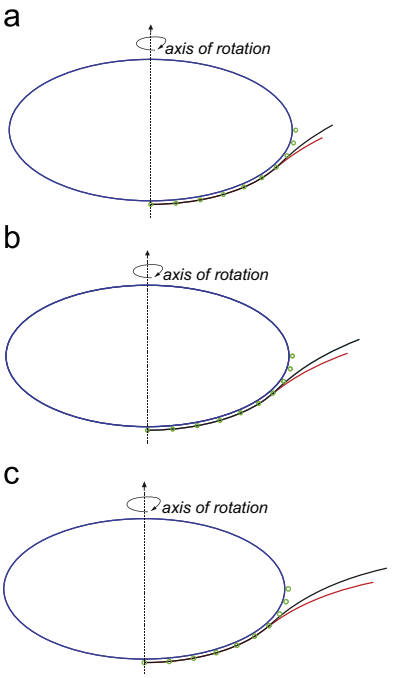

Fig. 10. The membrane profiles on ellipsoidal NP ($\lambda = 0.5$) for different adhesion strengths with vesicle size (a) $v = 3$, (b) $v = 5$, (c) $v = 10$ in which red line represent $\overline{\rho\varepsilon} = 541.7$ and black one represent $\overline{\rho\varepsilon} = 687.4$. This figure is for 3D case. (For interpretation of the references to color in this figure legend, the reader is referred to the web version of this article.)

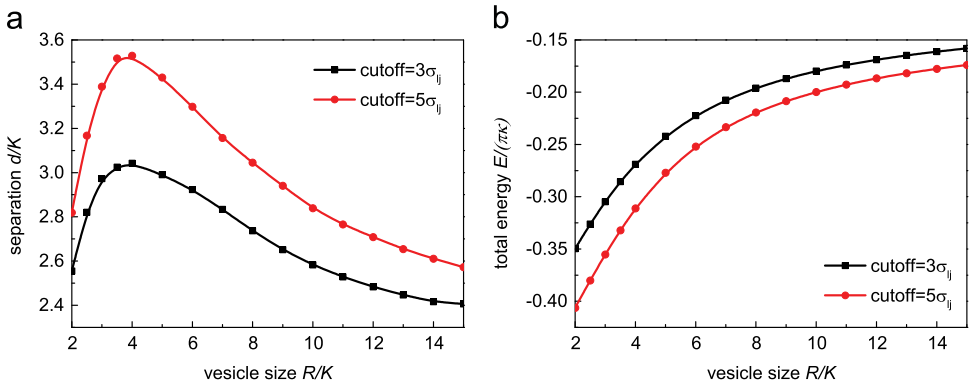

Fig. 11. Effects of the vesicle size on the separation (a) and total energy (b) with different cutoff distances. This figure is for 3D case.

shows the spherical NPs separation versus the vesicle size with different cutoff distance. It seems the increase of cutoff distance would influence the optimal separation distance (Fig. 11a) while showing minor effect on the energy gain (Fig. 11b).

3.5. Comparison with individual wrapping and cooperative tubular wrapping

Bahrami et al. (2012) and Saric and Cacciuto (2012a, 2012b) have studied the tube formation of multiple spherical NPs on vesicles. To see if such tubular cooperative entry is more energetically favorable than the spherical cooperative entry, we conduct the following comparison. Fig. 12a–c shows the membrane profiles for different wrapping models in which Fig. 12a shows the case when one NP is fully wrapped by the membrane, Fig. 12b shows the case when at equilibrium, individual NP is wrapped by the membrane and Fig. 12c shows the tubular cooperative entry of multiple NPs. In Fig. 12d we compare the energies for different entry modes at different parameters of $\bar{\sigma}$. For spherical cooperative entry, we set the vesicle size $R/K=\sqrt{2}$ and $\varphi=45^\circ$. It is seen that spherical cooperative entry of NPs can gain more energy compensation than individual wrapping when $\bar{\sigma}$ is smaller than 0.07. Since $\bar{\sigma}=\sigma K^2/\kappa$, it means NPs with a small size prefer to enter cell via cooperative mode. We note that for individual entry, the NP cannot be fully wrapped by the membrane, thus cannot be internalized into the cell. Meanwhile, we notice that tubular cooperative entry is more favorable than spherical cooperative entry of spherical NPs.

For oblate NPs, however, the total energy in tubular cooperative entry mode no longer prevails. Fig. 13a–c shows the membrane profiles at different entry modes. We compare the energies at different entry modes in Fig. 13d. It is seen that the system energies are significantly higher for the tubular cooperative entry than that for spherical cooperative entry. If the NPs were fully wrapped by the membrane, the system energies are even higher, as shown in Fig. 13d. It indicates that the spherical cooperative entry of oblate NPs is favorable compared to individual wrapping.

We also investigate how the aspect ratio λ influences the total energy of the tubular and spherical cooperative modes. According to our previous definition, the semi-major and semi-minor axis of an ellipsoid with different aspect ratio is shown in Table 5. As shown in Fig. 14a, the wrapping degree decreases as the aspect ratio decreases. And the spherical cooperative entry becomes energetic favorable at $\lambda=0.95$ (Fig. 14b), indicating the small change of the shape of NPs would alter the entry modes from tubular cooperative entry to spherical cooperative entry.

We note that in the tubular mode for oblate NPs, we only consider the case when neighboring NPs face each other via their less curved sides. Another possible mode is that the neighboring NPs face each other via their strong curved sides, which partially costs more bending energy while gains more adhesion energy. This entry mode is worthy to be further

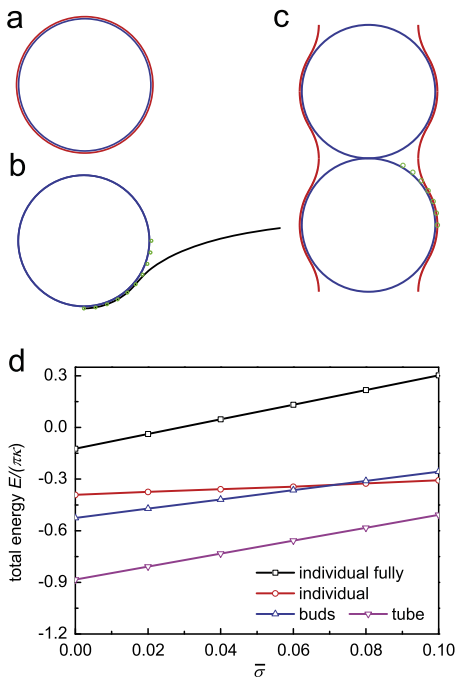

Fig. 12. (a) Schematic diagram of individual NPs wrapped by membrane completely. (b) The membrane profile for individual wrapping (black line) of NPs. The adhesion strength $\overline{\rho\varepsilon}=541.7$ and the dimensionless parameter $\bar{\sigma}=0.055$ are used. (c) The membrane profile for tubular cooperative entry of NPs. The parameters are the same as individual wrapping. (d) The relation between the total energy and the dimensionless parameter $\bar{\sigma}$ when cell internalizes NPs with different modes ($\bar{\sigma}=\sigma K^2/\kappa$). For spherical cooperative entry of NPs, we set the vesicle size $R/K=\sqrt{2}$ and $\varphi=45^\circ$. The black line represents the total energy when individual NP is fully wrapped by membrane. The red line represents the minimum energy when individual NP just adheres to the membrane. (For interpretation of the references to color in this figure legend, the reader is referred to the web version of this article.)

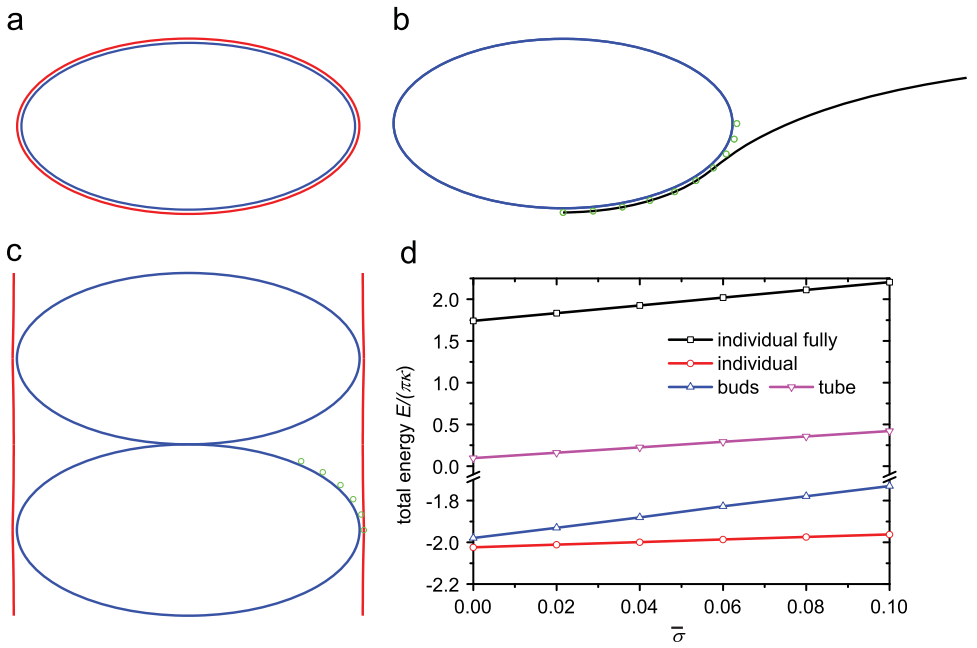

Fig. 13. (a) Schematic diagram of individual ellipsoidal NPs wrapped by membrane completely. (b) The membrane profile for individual wrapping (black line) of ellipsoidal NPs ($\lambda=0.5$). The adhesion strength $\overline{\rho\varepsilon}=541.7$ and the parameter $\bar{\sigma}=0.055$ are used. (c) The membrane profile for cooperative wrapping of ellipsoidal NPs in tubes. The parameters are the same as individual wrapping. (d) The relation between the total energy and the dimensionless parameter $\bar{\sigma}$ when cell internalizes ellipsoidal NPs with different modes ($\bar{\sigma}=\sigma K^2/\kappa$). For cooperative wrapping of NPs in spherical buds, we set the vesicle size $R/K=\sqrt{2}$ and $\varphi=45^\circ$. The black line represents the total energy when individual NP is fully wrapped by membrane. The red line represents the minimum energy when individual NP just adheres to the membrane. (For interpretation of the references to color in this figure legend, the reader is referred to the web version of this article.)

Table 5
Semi-major and semi-minor axis of an ellipsoid.

	$\lambda=0.5$	$\lambda=0.6$	$\lambda=0.7$	$\lambda=0.8$	$\lambda=0.9$	$\lambda=1$
a/K (3D)	1.260	1.186	1.126	1.077	1.036	1.000
b/K (3D)	0.630	0.711	0.788	0.862	0.932	1.000

investigated. However, this orientation is not rotationally symmetric, and thus beyond the scope of current methods. We would study it further elsewhere.

3.6. Discussions

In our cooperative entry model we only consider oblate ellipsoidal NPs with their flat side adhering to the membrane. It is more likely to form spherical vesicle to complete the internalization of multiple NPs. For prolate ellipsoidal NPs which initially adhere to membrane by their flat side, there is no rotational symmetry around the short axis (Bahrami, 2013), and our model would not work anymore. One alternative entry way is that the prolate NPs align in a row along their long axis and the membrane forms tube to internalize these NPs (Bahrami, 2013; Raatz et al., 2014; Saric and Cacciuto, 2012b). Such tubular entry model would avoid wrapping the strong curved tips of prolate NPs. In present paper, we have extended this model to investigate the internalization of spherical/ellipsoidal NPs by spherical vesicles, rather than tubular vesicles.

Recent works have shown that there are two modes for cellular entry of one-dimensional NP: the long axis of NPs is oriented parallel to the membrane or perpendicular to the membrane (Bahrami, 2013; Dasgupta et al., 2014; Huang et al., 2013; Shi et al., 2011; Yi et al., 2014). Generally upon contact, the NPs would adhere to the membrane by their flat side, and then it may adopt different entry modes depending on different situations. Our model is actually more suitable to describe the initial stage of cellular uptake NPs.

In one recent paper, the authors show that the elasticity of NPs plays significant role in cellular entry of soft NPs (Yi and Gao, 2014; Yi et al., 2011). They find that rigid NPs are easier to be fully wrapped by the cell membrane than the soft ones. The mechanism is that, during uptake, initially spherical NP would deform into ellipsoid due to the stretch of membrane, which prohibits its fully wrapping due to the high bending energy compensation. Considering the fact that ellipsoidal NPs

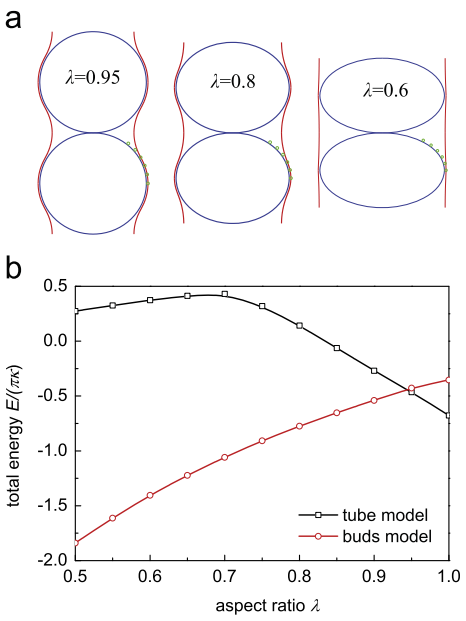

Fig. 14. (a) Membrane profiles for tubular structure with different aspect ratios. We set $\overline{\rho\varepsilon}=541.7$, $\overline{\sigma}=0.055$. (b) The effects of aspect ratio on the total energy for tube model and buds model. For spherical buds, we set $R/K=\sqrt{2}$ and $\varphi=45^{\circ}$, other parameters are the same as tubular mode.

get more energy gain than the spherical ones during cooperative entry, we propose that soft NPs should have advantages over rigid ones in cooperative entry.

4. Conclusions

In summary, we have set up a new model for cellular entry of multiple NPs. We consider different shapes of NPs, including spherical, ellipsoidal, cylindrical, elliptic cylindrical NPs. The model describes cellular entry of multiple NPs by spherical vesicle, which is more suitable for oblate/soft/small NPs. The effect of adhesion strength and the cutoff of potential are also discussed. Our work can be used to actively design and transfer NPs in applications such as drug delivery, imaging, and therapy in nanomedicine, as well as to understand the shape effect on toxic mechanism of ellipsoidal NPs. Although our model focuses on cellular uptake of NPs, it is also suitable to describe cellular budding NPs as well (Auth and Gompper, 2009). In addition, it may provide guideline for proteins aggregate on cell membrane (Haselwandter and Phillips, 2013; Simunovic et al., 2013).

Acknowledgments

The work is supported by the National Natural Science Foundation of China (NSFC) (Grants 11272327, 11422215 and 11023001), the Early Career Scheme (ECS) of Hong Kong RGC (Grant no. 533312) and the Internal Competitive Research Grants (A-PM24) from the Hong Kong Polytechnic University, and computation is mainly supported by the Supercomputing Center of Chinese Academy of Sciences (SCCAS). We thank the PhD student Wanye Xu from Xidian University for helpful discussions on numerical optimization and Prof. Yujie Wei from Institute of Mechanics, Chinese Academy of Sciences for helpful discussion and suggestion.

References

Agarwal, R., Singh, V., Jurney, P., Shi, L., Sreenivasan, S.V., Roy, K., 2013. Mammalian cells preferentially internalize hydrogel nanodiscs over nanorods and use shape-specific uptake mechanisms. Proc. Natl. Acad. Sci. USA 110, 17247–17252.
Auth, T., Gompper, G., 2009. Budding and vesiculation induced by conical membrane inclusions. Phys. Rev. E 80, 031901.
Bahrami, A.H., 2013. Orientational changes and impaired internalization of ellipsoidal nanoparticles by vesicle membranes. Soft Matter 9, 8642–8646.
Bahrami, A.H., Lipowsky, R., Weikl, T.R., 2012. Tubulation and aggregation of spherical nanoparticles adsorbed on vesicles. Phys. Rev. Lett. 109, 188102.
Bahrami, A.H., Raatz, M., Agudo-Canalejo, J., Michel, R., Curtis, E.M., Hall, C.K., Gradzielski, M., Lipowsky, R., Weikl, T.R., 2014. Wrapping of nanoparticles by membranes. Adv. Colloid Interface Sci. 208, 214–224.
Boal, D., 2012. Mechanics of the Cell, second ed. Cambridge University Press, Cambridge, UK.
Canton, I., Battaglia, G., 2012. Endocytosis at the nanoscale. Chem. Soc. Rev. 41, 2718–2739.
Champion, J.A., Mitragotri, S., 2006. Role of target geometry in phagocytosis. Proc. Natl. Acad. Sci. USA 103, 4930–4934.
Chaudhuri, A., Battaglia, G., Golestanian, R., 2011. The effect of interactions on the cellular uptake of nanoparticles. Phys. Biol. 8, 046002.

Chithrani, B.D., Chan, W.C.W., 2007. Elucidating the mechanism of cellular uptake and removal of protein-coated gold nanoparticles of different sizes and shapes. Nano Lett. 7, 1542–1550.
Chithrani, B.D., Ghazani, A.A., Chan, W.C.W., 2006. Determining the size and shape dependence of gold nanoparticle uptake into mammalian cells. Nano Lett. 6, 662–668.
Dasgupta, S., Auth, T., Gompper, G., 2013. Wrapping of ellipsoidal nano-particles by fluid membranes. Soft Matter 9, 5473–5482.
Dasgupta, S., Auth, T., Gompper, G., 2014. Shape and orientation matter for the cellular uptake of nonspherical particles. Nano Lett. 14, 687–693.
Davis, M.E., Chen, Z., Shin, D.M., 2008. Nanoparticle therapeutics: an emerging treatment modality for cancer. Nat. Rev. Drug Discov. 7, 771–782.
Decuzzi, P., Ferrari, M., 2008. The receptor-mediated endocytosis of nonspherical particles. Biophys. J. 94, 3790–3797.
Deserno, M., 2004. Elastic deformation of a fluid membrane upon colloid binding. Phys. Rev. E 69, 031903.
Doane, T.L., Burda, C., 2012. The unique role of nanoparticles in nanomedicine: imaging, drug delivery and therapy. Chem. Soc. Rev. 41, 2885–2911.
Florez, L., Herrmann, C., Cramer, J.M., Hauser, C.P., Koynov, K., Landfester, K., Crespy, D., Mailander, V., 2012. How shape influences uptake: interactions of anisotropic polymer nanoparticles and human mesenchymal stem cells. Small 8, 2222–2230.
Gao, H.J., 2014. Probing mechanical principles of cell–nanomaterial interactions. J. Mech. Phys. Solids 62, 312–339.
Gao, H.J., Shi, W.D., Freund, L.B., 2005. Mechanics of receptor-mediated endocytosis. Proc. Natl. Acad. Sci. USA 102, 9469–9474.
Gozdz, W.T., 2007. Deformations of lipid vesicles induced by attached spherical particles. Langmuir 23, 5665–5669.
Gratton, S.E.A., Ropp, P.A., Pohlhaus, P.D., Luft, J.C., Madden, V.J., Napier, M.E., DeSimone, J.M., 2008. The effect of particle design on cellular internalization pathways. Proc. Natl. Acad. Sci. USA 105, 11613–11618.
Haselwandter, C.A., Phillips, R., 2013. Directional interactions and cooperativity between mechanosensitive membrane proteins. Europhys. Lett. 101, 68002.
Helfrich, W., 1973. Elastic properties of lipid bilayers: theory and possible experiments. Z. Naturforsch. C 28, 693–703.
Huang, C.J., Zhang, Y., Yuan, H.Y., Gao, H.J., Zhang, S.L., 2013. Role of nanoparticle geometry in endocytosis: laying down to stand up. Nano Lett. 13, 4546–4550.
Jaskiewicz, K., Larsen, A., Lieberwirth, I., Koynov, K., Meier, W., Fytas, G., Kroeger, A., Landfester, K., 2012a. Probing bioinspired transport of nanoparticles into polymersomes. Angew. Chem. Int. Ed. 51, 4613–4617.
Jaskiewicz, K., Larsen, A., Schaeffel, D., Koynov, K., Lieberwirth, I., Fytas, G., Landfester, K., Kroeger, A., 2012b. Incorporation of nanoparticles into polymersomes: size and concentration effects. ACS Nano 6, 7254–7262.
Jiang, L.Y., Huang, Y., Jiang, H., Ravichandran, G., Gao, H., Hwang, K.C., Liu, B., 2006. A cohesive law for carbon nanotube/polymer interfaces based on the van der Waals force. J. Mech. Phys. Solids 54, 2436–2452.
Kennedy, J., Eberhart, R., 1995. Particle swarm optimization. In: Proceedings of IEEE International Conference on Neural Networks, New York.
Lewinski, N., Colvin, V., Drezek, R., 2008. Cytotoxicity of nanoparticles. Small 4, 26–49.
Morris, C.E., Homann, U., 2001. Cell surface area regulation and membrane tension. J. Membr. Biol. 179, 79–102.
Nel, A.E., Madler, L., Velegol, D., Xia, T., Hoek, E.M.V., Somasundaran, P., Klaessig, F., Castranova, V., Thompson, M., 2009. Understanding biophysicochemical interactions at the nano-bio interface. Nat. Mater. 8, 543–557.
Osaki, F., Kanamori, T., Sando, S., Sera, T., Aoyama, Y., 2004. A quantum dot conjugated sugar ball and its cellular uptake on the size effects of endocytosis in the subviral region. J. Am. Chem. Soc. 126, 6520–6521.
Qin, Z., Buehler, M.J., 2014. Molecular mechanics of mussel adhesion proteins. J. Mech. Phys. Solids 62, 19–30.
Raatz, M., Lipowsky, R., Weikl, T.R., 2014. Cooperative wrapping of nanoparticles by membrane tubes. Soft Matter 10, 3570–3577.
Reynwar, B.J., Deserno, M., 2011. Membrane-mediated interactions between circular particles in the strongly curved regime. Soft Matter 7, 8567–8575.
Reynwar, B.J., Illya, G., Harmandaris, V.A., Muller, M.M., Kremer, K., Deserno, M., 2007. Aggregation and vesiculation of membrane proteins by curvature-mediated interactions. Nature 447, 461–464.
Saric, A., Cacciuto, A., 2012a. Fluid membranes can drive linear aggregation of adsorbed spherical nanoparticles. Phys. Rev. Lett. 108, 118101.
Saric, A., Cacciuto, A., 2012b. Mechanism of membrane tube formation induced by adhesive nanocomponents. Phys. Rev. Lett. 109, 188101.
Shi, X.H., von dem Bussche, A., Hurt, R.H., Kane, A.B., Gao, H.J., 2011. Cell entry of one-dimensional nanomaterials occurs by tip recognition and rotation. Nat. Nanotechnol. 6, 714–719.
Simunovic, M., Srivastava, A., Voth, G.A., 2013. Linear aggregation of proteins on the membrane as a prelude to membrane remodeling. Proc. Natl. Acad. Sci. USA 110, 20396–20401.
Slowing, I.I., Vivero-Escoto, J.L., Wu, C.W., Lin, V.S.Y., 2008. Mesoporous silica nanoparticles as controlled release drug delivery and gene transfection carriers. Adv. Drug Deliv. Rev. (60), 1278–1288.
Verma, A., Stellacci, F., 2010. Effect of surface properties on nanoparticle–cell interactions. Small 6, 12–21.
Wang, J.L., Wei, Y.J., Shi, X.H., Gao, H.J., 2013. Cellular entry of graphene nanosheets: the role of thickness, oxidation and surface adsorption. RSC Adv. 3, 15776–15782.
Yang, K., Ma, Y.Q., 2010. Computer simulation of the translocation of nanoparticles with different shapes across a lipid bilayer. Nat. Nanotechnol. 5, 579–583.
Yi, X., Gao, H.J., 2014. Phase diagrams and morphological evolution in wrapping of rod-shaped elastic nanoparticles by cell membrane: a two-dimensional study. Phys. Rev. E 89, 062712.
Yi, X., Shi, X.H., Gao, H.J., 2011. Cellular uptake of elastic nanoparticles. Phys. Rev. Lett. 107, 098101.
Yi, X., Shi, X.H., Gao, H.J., 2014. A universal law for cell uptake of one-dimensional nanomaterials. Nano Lett. 14, 1049–1055.
Yue, T.T., Zhang, X.R., 2012. Cooperative effect in receptor-mediated endocytosis of multiple nanoparticles. ACS Nano 6, 3196–3205.
Zhang, S.L., Li, J., Lykotrafitis, G., Bao, G., Suresh, S., 2009. Size-dependent endocytosis of nanoparticles. Adv. Mater. 21, 419–424.